



HAL
open science

Sub-picosecond dynamic of intense laser-clusters interaction: keV X-ray and highly charged ions production

Emily Lamour, S. Dreuil, J.-C. Gauthier, Olivier Gobert, Pierre Meynadier, Didier Normand, Michel Perdrix, Christophe Prigent, Jean Marc Ramillon, Jean-Pierre Rozet, et al.

► To cite this version:

Emily Lamour, S. Dreuil, J.-C. Gauthier, Olivier Gobert, Pierre Meynadier, et al.. Sub-picosecond dynamic of intense laser-clusters interaction: keV X-ray and highly charged ions production. Applications of X Rays Generated from Lasers and Other Bright Sources II - SPIE 2001, 2001, San Diego, United States. pp.97-105, 10.1117/12.448454 . hal-00008291

HAL Id: hal-00008291

<https://hal.science/hal-00008291>

Submitted on 31 Aug 2005

HAL is a multi-disciplinary open access archive for the deposit and dissemination of scientific research documents, whether they are published or not. The documents may come from teaching and research institutions in France or abroad, or from public or private research centers.

L'archive ouverte pluridisciplinaire **HAL**, est destinée au dépôt et à la diffusion de documents scientifiques de niveau recherche, publiés ou non, émanant des établissements d'enseignement et de recherche français ou étrangers, des laboratoires publics ou privés.

Sub-picosecond dynamic of intense laser-clusters interaction : keV X-ray and highly charged ions production[¶]

E. Lamour^{a*}, S. Dreuil^a, J-C. Gauthier^b, O. Gobert^c, P. Meynadier^c, D. Normand^c, M. Perdrix^c,
C. Prigent^a, J.M. Ramillon^d, J-P. Rozet^a, and D. Vernhet^a

^a Groupe de Physique des Solides, CNRS UMR 75-88, Universités Paris 7 et Paris 6, 75251 Paris Cedex 05, France; ^b LULI, CNRS UMR 7605, Ecole Polytechnique, 91128 Palaiseau Cedex, France; ^c CEA-Saclay, DSM/DRECAM/SPAM Bât. 522, 91191 Gif-sur-Yvette Cedex, France; ^d CIRIL, UMR 11 CNRS-CEA, BP 5133, 14070 Caen Cedex 5, France

ABSTRACT

We have performed studies of keV X-ray production from $(Ar)_n$, $(Kr)_n$ and $(Xe)_n$ rare gas clusters (with n between 10^4 and 10^6 atoms/cluster) submitted to intense ($\leq 10^{18}$ W/cm²) infrared (800 nm) laser pulses. Up to 10^6 3 keV photons per pulse at a moderate (10^{15} /cm³) atomic density have been observed. High resolution spectroscopy studies in the case of $(Ar)_n$ clusters have also been performed, giving unambiguous evidence of highly charged (up to heliumlike) ions with K vacancies production. We have determined the photon energies and the absolute photon emission yields as a function of several physical parameters governing the interaction : size and atomic number of the clusters, peak intensity of the laser. Unexpectedly low laser intensity thresholds ($\approx 10^{15}$ Wcm⁻²) have been measured. The results obtained indicate nevertheless that X-rays may be emitted before cluster explosion on a subpicosecond time scale, and that several mechanisms must be involved in the first stage of the production of the hot nanoplasma induced from each cluster.

Keywords: Intense laser pulses, clusters, X-rays, highly charged ions

1. INTRODUCTION

A current subject of interest is the possibility of constructing cheap versatile sources producing intense and/or short X-ray pulses for applications. Table-top devices are now available that can produce subpicosecond laser pulses with intensities easily exceeding 10^{18} W/cm². This has opened a new area in the field of laser-matter interaction, including the generation of high order harmonics in the UV range, high charge states and keV X-rays using clusters or solids. Cluster targets have received considerable attention in recent years for several reasons. In the first place, they allow to study matter behavior in the gap between solid and gaseous targets, they offer the opportunity of observing well isolated *nanoplasmas*, and constitute simple objects where laser-matter interaction may be understood and modeled more easily. Second, they constitute renewable targets free of debris and can nevertheless be very efficient in absorbing laser energy, and may then be a very convenient tool to produce intense X-rays and fast electrons as well as highly charged ions. Hot electrons with energies of a few keV¹ and multicharged ions with energies reaching the MeV have been observed^{2,3,4,5}. Up to now, X-ray emission studies have been mainly limited to qualitative observations and theoretical discussions^{6,7,8,9,10,11,12,13}, but a critical analysis of the predictions of various models which have been proposed in terms of experimental observables is still lacking. We are conducting a systematic research program to measure absolute X-ray emission yields and ionic charge state distributions as a function of various physical parameters governing the laser-cluster interaction : these parameters include the cluster size, atomic number and total atomic density on one hand, and the laser pulse energy, pulse duration, wavelength and polarization on the other hand. Results relative to cluster size and atomic number, and to laser pulse energy are presented here. Two main series of measurements have been conducted. The first series were obtained in a high laser intensity regime, and a simple inner-shell ionization model was elaborated, reproducing well our observations. As will be shown, this model predicts a threshold behavior, which has been examined in a second series of measurements. This second series were obtained in a low intensity regime, using a different experimental set-up. Only preliminary results corresponding to this very

[¶] Experiment performed at LUCA-SPAM/DRECAM/DSM CEA-Saclay

* lamour@gps.jussieu.fr, phone 33 1 44 27 45 18; fax 33 1 44 27 73 09

recent study are reported here. The observed laser intensity thresholds are nevertheless much lower than expected, thus bearing evidence for new highly non linear phenomena neglected so far.

2. EXPERIMENTAL SETUP

The experimental set-up, including the apparatus used for cluster generation and the X-ray spectrometers, has been described in detail in previous publications^{4,9,14}. Briefly, clusters are generated within a pulsed adiabatic expansion of the well documented Hagen type¹⁵. This device leads to a mean cluster size \tilde{N}_c given by

$$\tilde{N}_c \approx A_c P_0^{1.95}, \quad (1)$$

where P_0 is the backing pressure (bar) and A_c is a quantity depending on the atomic species, the temperature and the geometry of the nozzle. In our case, A_c amounts to $2.1 \cdot 10^3$, $6.7 \cdot 10^3$ and $2.3 \cdot 10^4$ respectively for Ar, Kr and Xe species. The atomic beam density ρ_c at a working distance from the nozzle of 475 mm follows a linear dependence on the backing pressure given by

$$r_c \gg 5 \times 10^{13} P_0 \text{ cm}^{-3}. \quad (2)$$

The intense laser field is generated with a Ti:sapphire laser system delivering pulses of minimum duration of 60fs at 800 with a repetition rate of 20Hz. The beam diameter is approximately 45mm and the maximum pulse energy available in the interaction zone is 90mJ.

In the case of high intensity results, laser pulses of 80 to 130fs duration are used, and the laser light is focused with a $f=170\text{mm}$ off-axis parabola leading to a maximum peak intensity $I_{peak}^{max} \sim 10^{18} \text{Wcm}^{-2}$. The I_{peak} values are determined from the saturation intensities in the optical field ionization (OFI) of a low density atomic neon target using the barrier suppression ionization model (BSI)¹⁶, and correspond to a $1/e^2$ diameter $\sim 12\mu\text{m}$. The precision of this method is estimated to be $\pm 20\%$.

For low intensity studies, the working distance from the nozzle is 500 mm and we use a $f=480$ mm lens : the focal spot was imaged with a CCD camera and its $1/e^2$ diameter found to be $43(\pm 3)\mu\text{m}$. Pulses of 60fs duration and with a maximum energy of 60mJ have been used, leading to peak intensities in the range $10^{15} - 7.10^{16} \text{Wcm}^{-2}$.

The X-rays are analyzed using two Si(Li) detectors and a crystal spectrometer. The Si(Li) detectors are sealed with thin ($25\mu\text{m}$) Be windows and can be placed at different angles (0° , 100° and 145°) with respect to the laser beam. To reduce the counting rates of these very efficient detector systems (typical solid angle of detection of $\sim 5 \times 10^3$ sr), we use small apertures and/or thin aluminum-coated Mylar foils. For low counting rates, a single peak is observed at the characteristic energy of the observed atomic transition (“one-photon spectrum”); for higher counting rates, several photons are detected within one laser shot, and pileup occurs : peaks at two, three, four... times the energy of the single photon peak are observed, obeying a Poisson distribution; finally, for very high counting rates, a Gaussian peak is observed, whose position is proportional to both the photon energy and the detected number of photons per pulse. This effect is illustrated in figure 1 in the case when the observed transition is the X_L line of Kr^{q+} of ~ 1.75 keV energy.

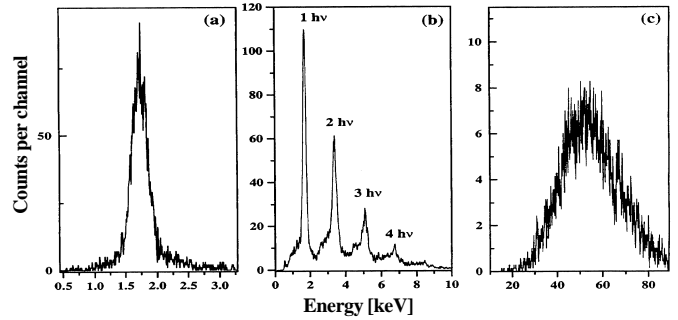


Figure 1. X-ray spectra obtained during irradiation of krypton clusters. Spectrum (a) is recorded at a very low counting rate (much less than one detected photon per laser pulse) by using a diaphragm in front of the detector, spectrum (b) corresponds to an average of about one detected photon per laser pulse and spectrum (c) to a large counting rate (about 30 detected photons per pulse).

State resolved measurements are performed using a high-resolution high-transmission Bragg-crystal spectrometer equipped with a flat mosaic graphite crystal (HOPG) and a position sensitive detector working in the photon counting mode. Typical integrated efficiency and resolving power of this spectrometer are respectively $2 \cdot 10^{-6}$ and 2000.

3. HIGH INTENSITY RESULTS

We first present the absolute photon yields measured with the Si(Li) detectors for Ar, Kr and Xe clusters. More detailed information obtained with the crystal spectrometer are presented in the next subsection.

3.1 Low resolution results

Systematic studies of the emission pattern have been performed using three different arrangements of the positions of the two Si(Li) detectors⁹. In all cases, an isotropic emission pattern is observed within the experimental error of $\pm 5\%$. Similarly, no dependence on the orientation of the polarization vector of the laser light has been found. The absolute photon yield can then be extracted from the total counts observed in any of our detectors of known detection efficiency and the simultaneously recorded number of laser pulses. Typical one-photon spectra corresponding to Ar, Kr and Xe clusters are given in figure 2.

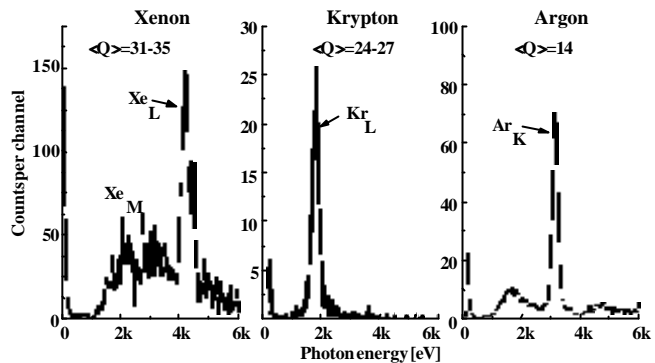


Figure 2. One-photon spectra recorded during irradiation of argon, krypton and xenon clusters under similar conditions (130fs infrared pulses at 800nm with a peak intensity of $5 \times 10^{17} \text{ W cm}^{-2}$ and a backing pressure of 18bar).

K-shell ionization of argon and L-shell ionization of krypton and xenon are observed. Studies of the X-ray yield dependence on laser peak intensity have been performed using Si(Li) detectors in the case of $(\text{Ar})_n$ and $(\text{Kr})_n$ clusters, leading to identical scaling laws.

Since an extensive study on both the laser peak intensity and the backing pressure has been done and more results obtained in the case of Ar high-resolution spectroscopy, the corresponding results will be given in the next subsection. We only give here quantitative results on the atomic species dependence, with measurements performed at the same (18 bar) backing pressure and laser peak intensity ($5 \times 10^{17} \text{ W cm}^{-2}$). Results are summarized in Table 1.

	argon	krypton	xenon
E_{hv} (eV)	3086	1741/2248	4109
N_{hv} / pulse	7×10^4	4×10^6	1.5×10^5
$\langle Q \rangle$	14	24-27	31-35

Table 1. Energies, photon yields (total photon number in $4\pi \text{ sr}$ per laser pulse) and mean charge states extracted in the case of argon, krypton and xenon clusters for the same (18 bar) backing pressure and laser peak intensity of $5 \times 10^{17} \text{ W cm}^{-2}$.

The highest yield is obtained with krypton clusters. The observed low-resolution spectrum is in good agreement with the high-resolution spectrum observed by McPherson *et al.*⁷. With the geometry and the backing pressure used here, the atomic density in the interaction region is only $9 \times 10^{14} \text{ cm}^{-3}$, whereas densities 5 orders of magnitude larger can easily be obtained by working at higher pressure and closer to the gas jet nozzle. For such densities, the photon yield would be in excess of 10^{11} $\sim 2 \text{ keV}$ photons / pulse! The lowest yield corresponds to the argon case, and xenon is in between. At this stage, it is already worth noting that the observed mean charge states (deduced from X-ray energies^{17,18}) are much larger than those corresponding to direct observation of ionic species from the cluster after explosion^{2,5}. For instance, Lezius *et al.*⁴ have reported *maximum* charge states corresponding to Ar^{10+} and Xe^{30+} in similar conditions. In such a case, however, highly charged ions are in fact detected well after the early inner-shell ionization stage under examination here, and certainly after some recombination has occurred with surrounding electrons.

3.2 High resolution results

3.2.1 High resolution spectra

Though the observed yields are not as large in the case of argon as with other cluster targets, the observed X-ray transitions have here a relatively simple character : it is expected that mainly $1s2p2l^n \rightarrow 1s^22l^n$ transitions must be present in a high resolution spectrum, thus simplifying its interpretation (we note also that no significant contribution of $K\beta$ transitions are found in the Si(Li) spectra in this case, meaning that almost no M shell electrons are present at the time of K-shell X-ray emission). This is actually the case, as observed in the sample spectrum presented in figure 3 corresponding to near optimum conditions, the working distance from the nozzle being however kept to 475 mm (backing pressure $P_0 = 30$ bar, laser pulses of 80fs duration with a peak intensity of $6.7 \times 10^{17} \text{ W cm}^{-2}$).

$1s2p2l^n \rightarrow 1s^22l^n$ transitions with $0 \leq n \leq 4$ corresponding to charge states $12+ - 16+$ are observed, with a prominent and well separated peak corresponding to the 1P_1 transition in heliumlike argon. Since no hydrogenlike transition was observed, the 1P_1 line is free of satellites; its width, however, is found to be 4.5 eV, whereas the instrumental one is 1.5 eV only. Hence, this line width is due to physical processes (such as Stark and/or Doppler broadening for instance), and may be used to diagnose the cluster-sized nanoplasma at the time when X-ray emission occurs. Several spectra similar to this one have been recorded for various backing pressures and laser peak intensities.

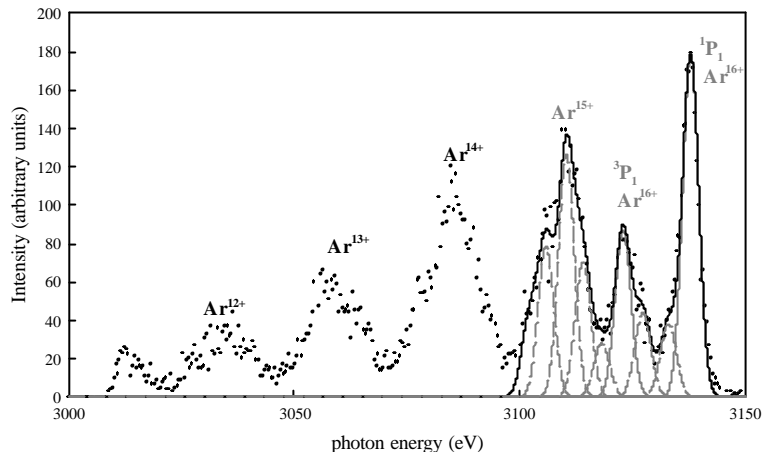


Figure 3. High-resolution spectrum recorded during irradiation of argon clusters by 80fs infrared pulses at 800nm with a peak intensity of $6.7 \times 10^{17} \text{ W cm}^{-2}$ and a backing pressure of 30bar.

3.2.2 Spectrum modelization

Some qualitative information can be deduced from the above spectrum. We have added to figure 3 a tentative fit of the relatively simple high-energy region of our spectrum (Ar^{16+} and Ar^{15+} lines) by including only transitions from $1s2p2l^n$ states with lifetimes not exceeding the laser pulse duration (~ 100 fs). Such a fit reflects well the observation. This agreement can be understood if we assume that K-shell ionization and X-ray emission occur on a similar, sub-picosecond scale, before cluster explosion. In that case, the electronic density must remain large at that time. On the other hand, this means that the electron mean energy (“temperature”) must be too small to (further) K-shell ionize the ions originating from the irradiated cluster. This temperature may nevertheless be already large enough¹ to induce some additional L-shell ionization, and certainly large enough to induce collisional mixing between various ionic configurations. These processes must be included in any model that would try to reproduce the relative intensities of the many (and often not well separated) lines in our spectra, in particular for the species with $q \leq 14$.

Such a more sophisticated model has been applied, and confirms these assumptions. We have used the HULLAC¹⁹ code as a data base for a *collisional-radiative* model solving the time evolution of populations due to competing processes such as collisional excitation and ionization, dielectronic recombination, autoionization and radiative processes. A stationary thermal distribution of electrons has been assumed. The electronic temperature T_e and the electronic density n_e , as well as the initial relative charge state fractions, have been adjusted to get the best fit. Also, the same broadening, as observed on the 1P_1 line, was applied to all transitions. The result of our calculation gives satisfactory agreement with experiment (figure 4) for $T_e = 750 \text{ eV}$ and $n_e = 10^{21} \text{ cm}^{-3}$. The extracted value for the electron temperature gives the mean kinetic energy acquired by ionized electrons at the time of X-ray emission, as a result of various processes such as inverse bremsstrahlung and electron-ion collisions. Electron energies are large enough to seriously affect the relative population of various excited substates and charge state fractions. This is illustrated in figure 4, where we have added a curve obtained by artificially inhibiting collisional excitation and ℓ -mixing processes.

However, this thermal energy is much lower than the laser-driven mean electron oscillation energy, and also too small to lead to further K-shell ionization. Assuming 14 free electrons per cluster atom, in concordance with the observed mean charge state of Ar ions at the time of X-ray emission, the extracted electronic density corresponds to an increase in the cluster radius of a factor of ~ 6 . This relatively small factor indicates that X-ray emission indeed takes place before cluster explosion, that is within at most a few hundreds femtoseconds. This conclusion is also supported by a simple inner-shell ionization model, based on the laser-driven electronic motion, that will be presented in section 4.

More complete numerical simulations including this inner-shell ionization stage and following the time evolution of the electron distribution function are in progress.

3.3 Laser energy and backing pressure dependence

In each case, we have deduced the total X-ray yields (photon number per pulse) from both the high resolution spectrum and the simultaneously recorded Si(Li) spectra. The mean photon energy, reflecting the mean charge state $\langle Q \rangle$ of the K-shell ionized emitting ions, was also deduced with high accuracy from the high resolution spectrum. Results, corresponding to the laser energy dependence, and the backing pressure one, are given respectively in figure 5 and 6.

The laser energy dependence is well fitted by a power law where the photon yield, N_{hn} , varies with the laser energy, or equivalently, the laser peak intensity, I_{peak} , as

$$N_{hn} \propto I_{peak}^{3/2}. \quad (3)$$

Such a behavior has been observed previously in experiments concerning OFI of rare-gas atoms¹⁶. These studies have shown that, as soon as the ion yield of a given charge state enters the saturation regime, the signal increases further with $I_{peak}^{3/2}$. This behavior is simply due to the increase with I_{peak} of the *effective focal volume* where a given threshold intensity is reached. Our result indicates that the process of inner-shell ionization is already saturated even at the lowest laser peak intensity used here ($\sim 1.7 \times 10^{17} \text{ W cm}^{-2}$). It can then be expected that the onset of the X-ray generation should occur at even lower intensities. Note that in the case of krypton cluster, X-ray emission is similarly observed⁹ for laser peak intensities down to $\sim 4 \times 10^{16} \text{ W cm}^{-2}$. The fact that the mean photon energy does not vary with the laser energy is also consistent with this picture : for a given cluster size, the ionization probabilities in K and L shells are constant inside a given, laser-intensity dependent, volume.

Whereas for a given backing pressure P_0 all spectra look the same, this is not the case when the cluster size is allowed to vary by varying P_0 : a distinct dependence of the mean photon energy on the backing pressure is found here (figure 6). Note that this energy variation has to be taken into account to extract the photon yields with the Si(Li) detectors, and much more accurate results are in fact obtained here using the high-resolution spectra. Analysis of the photon yield data indicate that the experimental result is best fitted with

$$N_{hn} \propto (P_0 - P_{min})^{5/3} \quad (4)$$

P_{min} is found in these measurements equal to 8bar, corresponding to a cluster size of $\sim 10^5$ atoms/cluster. As will be shown now, equation (4) is consistent with a model in which X-ray emission occurs following electron impact ionization inside each isolated cluster in the focal volume.

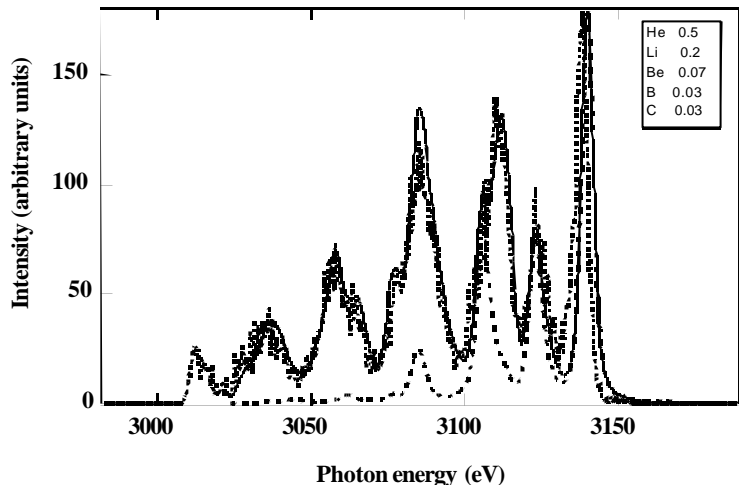


Figure 4. Comparison of the high-resolution argon spectrum with the HULLAC-based *collisional-radiative* simulation (smooth line). The broken line corresponds to the case when collisions are inhibited (see text), and the insert gives the initial charge state fractions.

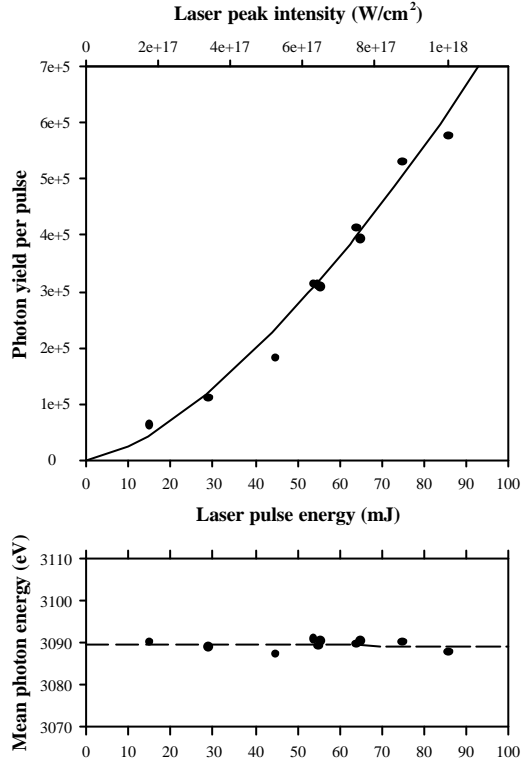


Figure 5. Argon cluster photon yield (upper plot) and mean photon energy (lower plot) dependence on the laser pulse energy recorded for 80fs pulses and a backing pressure of 26bar. The solid line in the upper plot is a fit with a power law of the form $E_{\text{laser}}^{3/2}$.

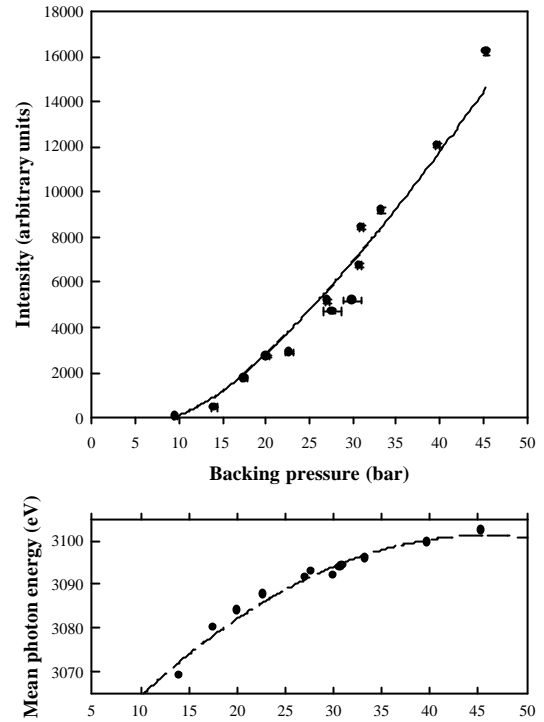


Figure 6. Argon cluster photon yield (upper plot) and mean photon energy (lower plot) dependence on the backing pressure recorded for 80fs pulses and a laser pulse energy of 90mJ. The solid line in the upper plot is a fit with a power law of the form $P_0^{5/3}$ where P_0 is the backing pressure.

4. INNER-SHELL IONIZATION MODEL

4.1 Inner-shell ionization scenario

We first consider the case of argon clusters with the experimental conditions of table 1 (backing pressure $P_0 = 18\text{bar}$ and 130fs laser pulses with a peak intensity $I_{\text{peak}} = 5 \times 10^{17} \text{ W cm}^{-2}$). We assume the following scenario :

- at an early stage of the laser-cluster interaction, OFI of argon atoms occurs, producing Ar^{8+} ions (Ne-like) and 8 quasi-free electrons. The threshold intensity for this process, for isolated atoms or ions, is estimated to be $2.6 \times 10^{16} \text{ W cm}^{-2}$, whereas producing Ar^{9+} requires peak intensities exceeding $1.6 \times 10^{18} \text{ W cm}^{-2}$, which is beyond the peak intensities of our experiment. Assuming a \sin^2 time dependence for the laser intensity, Ar^{8+} ions are produced at least 110fs before the peak intensity.
- later on, inner-shell ionization results from ionization and excitation processes induced by collisions between fast electrons and ionic species inside each isolated cluster. We consider that at this stage, very few electrons have already left the cluster by free streaming⁸, and that only laser driven electrons may have sufficient energy to produce argon K shell vacancies. This heating process has recently been shown²⁰ to explain multiple ionization even in the case of Ne atoms. Taking a 4 keV threshold for this process, a mean oscillation energy corresponding to this value is achieved for intensities of the order of $7 \times 10^{16} \text{ W cm}^{-2}$, about 100fs before the peak intensity. From then on, the effective focal volume (inside which this energy is achieved – see discussion after equation 3), starts to increase, and reaches about 5 times the nominal focal volume at the peak intensity. In between, about 38 optical cycles have taken place.

- at the time when the peak intensity is reached, some increase in the cluster radius has already taken place. Numerical simulations²¹ have shown that in the case considered here, the mean cluster radius has already increased by a factor of ~ 3 . It starts at that time to increase further very rapidly, and thus the collisional rate drops very fast (see below – equation 5). We then consider that no significant inner-shell ionization can take place after that time. This assumption is also consistent with the fact that the *collisional-radiative* simulation presented in section 3.2.2 above gives an electronic density corresponding to a relatively modest increase of the cluster radius at X-ray emission time.

Accordingly, the mean K-shell ionization number of argon atoms per laser pulse is given by

$$N_K = N_{\text{cycle}} n_e n \sigma x N_{\text{ag}}, \quad (5)$$

where $N_{\text{cycle}} = 38$ is the useful number of optical cycles, n_e is the number of laser driven electrons in each cluster, $n = 1/d^3$ is the atomic density inside the cluster (and d is the mean inter-atomic distance), σ is the electron-induced K-shell ionization cross section, x is the effective cluster thickness averaged over an optical cycle and N_{ag} is the total number of clusters in the effective focal volume. We take $n_e = 8 \tilde{N}_c$ (8 “free” electrons per cluster atom) and $d = 2 d_0$, allowing for some cluster expansion. $d_0 = 0.382\text{nm}$ is the mean inter-atomic distance in the cluster for atoms in their ground state. The K-shell ionization cross section²² is in the range $1\text{-}3 \times 10^{-21} \text{cm}^2$ for electron energies 4-50 keV, and we take as a mean value $\sigma = 2 \times 10^{-21} \text{cm}^2$. For a backing pressure $P_0 = 18\text{bar}$, $\tilde{N}_c = 5.9 \times 10^5$ and the initial cluster radius is equal to $\sim 20\text{nm}$. At a laser intensity of $7 \times 10^{16} \text{W cm}^{-2}$, the amplitude of the electron oscillations in the laser field is 22nm, a value very close to the cluster radius, and reaches 60nm at the peak intensity. We take $x = 40\text{nm}$ (the expanded cluster radius) as an order of magnitude. Finally, to evaluate the number of clusters in the effective focal volume, we take its time-averaged value which amounts to $\sim 2 V_{\text{foc}}$. The nominal focal volume, deduced from our laser intensity measurements, is $V_{\text{foc}} = 1.6 \times 10^{-8} \text{cm}^3$. With $\rho_c = 9 \times 10^{14} \text{cm}^{-3}$, we get $N_{\text{ag}} \sim 50$.

This gives $N_K \sim 1.6 \times 10^5$. Taking finally a mean fluorescence yield $\tilde{\omega}_K = 0.35$ deduced from the observed charge state distribution¹⁷, we predict an absolute photon yield/pulse of 6×10^4 , in good agreement with our experimental value of 7×10^4 (see table 1 and table 2 in next subsection).

4.2 Scaling laws : peak intensity, pressure and atomic species dependence

We first note that the inclusion of an inner-shell ionization threshold, taken to be here $\sim 7 \times 10^{16} \text{W cm}^{-2}$ in the case of argon, leads immediately to the observed laser energy dependence (equation 3). This threshold would be $\sim 3.5 \times 10^{16} \text{W cm}^{-2}$ for krypton. Unfortunately, in both cases, these values lie slightly under the lower intensities we have used in this first series of measurements. In fact, we will see in the next section that these thresholds have much lower values than expected.

Besides, ingredients in equation (5) obey the following scaling laws :

$$n_e = n_{\text{OFI}} \tilde{N}_c \approx n_{\text{OFI}} A_c P_0^2$$

$$n \propto d^{-3}$$

$$x \propto (\tilde{N}_c)^{1/3} d \propto A_c^{1/3} P_0^{2/3} d$$

$$N_{\text{ag}} \propto V_{\text{foc}}(I_s) \rho_c / \tilde{N}_c \propto V_{\text{foc}}(I_s) (A_c P_0)^{-1}$$

This leads to

$$N_K \propto n_{\text{OFI}} \sigma A_c^{1/3} P_0^{5/3} d^{-2} V_{\text{foc}}(I_s), \quad (6)$$

where A_c is defined in equation (1), n_{OFI} is the number of electrons initially released by OFI, and $V_{\text{foc}}(I_s)$ is the effective focal volume depending on the appropriate threshold electron energies.

First, one retrieves within this model the observed $P_0^{5/3}$ dependence for $(\text{Ar})_n$ clusters.

The atomic species dependence is contained in n_{OFI} , σ , A_c , d , $V_{\text{foc}}(I_s)$ and in the effective fluorescence yields when converting to photon yields. Estimated values of these quantities and predicted yields are given in table 2.

	argon	krypton	xenon
n_{OFI}	8	8	12
σ (10^{-21} cm ²)	2	8	2
A_c ($\times 10^3$)	2.1	6.7	23
d (nm)	0.764	0.412	0.456
$V_{\text{foc}}(I_s)$ (cm ³)	3.2×10^{-8}	7.4×10^{-8}	2.2×10^{-8}
$N_{\text{hv}} / \text{pulse}$	6×10^4 (7×10^4)	3×10^6 (4×10^6)	4×10^5 (1.5×10^5)

Table 2. OFI released electron numbers, ionization cross sections, scaling parameters for cluster size, mean inter-atomic distances in cluster, effective focal volumes and predicted photon yields, i.e. total photon number in 4π sr per laser pulse (experimental values quoted in Table 1 are given in parenthesis), for argon, krypton and xenon clusters for the same (18 bar) backing pressure and laser peak intensity of 5×10^{17} W cm⁻².

In our estimates, we have kept the krypton and xenon inter-atomic distances to their normal-cluster value, since cluster expansion is expected to occur later in these cases²⁰. Also, we have used here the same effective fluorescence yield as in the case of Ar; even if this quantity is much harder to calculate for L-shell transitions, this value corresponds to a right order of magnitude. This leads to an additional uncertainty in our estimates of a factor of about 2. Comparison between our calculations, given in table 2, with the experimental yields of table 1, shows nevertheless that the agreement is surprisingly good.

5. LOW INTENSITY RESULTS

New experiments have been performed to further test the laser intensity threshold behavior embedded in our model. Preliminary results of measurements conducted for both argon and krypton clusters are presented in figure 7 and 8.

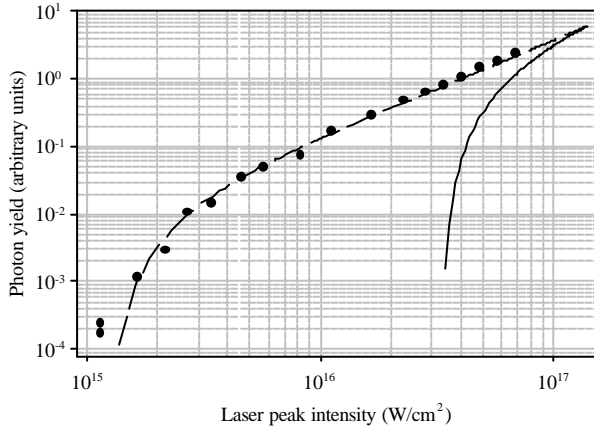


Figure 7. Argon cluster photon yield dependence on the laser peak intensity recorded for 60fs pulses and a backing pressure of 40bar. The solid line and the dashed line are the predictions of our model for threshold intensities of 3.5×10^{16} and 1.25×10^{15} W cm⁻² respectively. Model predictions have been arbitrarily normalized to experiment (see text).

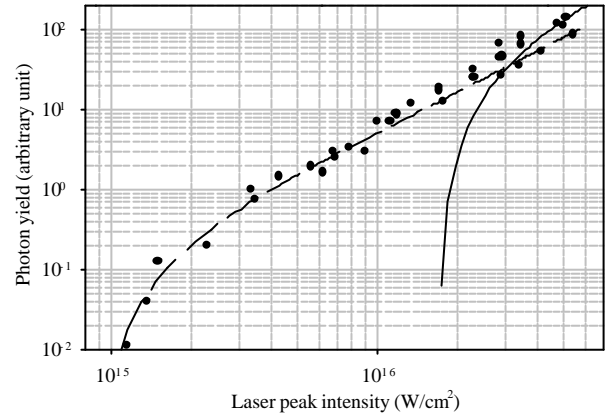


Figure 8. Krypton cluster photon yield dependence on the laser peak intensity recorded for 60fs pulses and a backing pressure of 12bar. The solid line and the dashed line are the predictions of our model for threshold intensities of 1.7×10^{16} and 1.0×10^{15} W cm⁻² respectively. Model predictions have been arbitrarily normalized to experiment (see text).

In both cases, a clear threshold is observed; these thresholds, however, correspond to much lower laser intensities than expected. The solid lines in figure 7 and 8 have been calculated using our model and a threshold intensity corresponding in each case to a *maximum* electron oscillation energy equal to the ionization energy (4 keV and 2 keV respectively). This is already a factor of two lower than what was assumed in our previous calculations (section 4.2), where the *mean* oscillation energy was considered. In fact, in both cases, the experiment is well fitted by our model if we assume a threshold intensity close to 10^{15} W cm⁻². A detailed data analysis must be performed before reaching a quantitative comparison of the absolute yields with our model predictions, on one hand, and with our previous high intensity measurements (section 3), on the other

hand. Model predictions in figure 7 and 8 have been arbitrarily normalized to experiment in the $\hat{I}^{1/2}$ region (saturation regime). At present, we can just speculate on the existence of a possible mechanism that would explain our finding. In the nanoplasma model⁸, it is expected that an enhancement of the field inside the cluster by several orders of magnitude, must take place when the cluster electronic density matches 3 times the critical density given by

$$n_c \approx 1.11 \times 10^{21} I^{-2}, \quad (7)$$

with n_c in cm^{-3} and λ in μm . This happens just before the cluster radius starts to increase very rapidly ; numerical simulations show, however, that the electronic “temperature” is increased during a short time only (~ 1 optical cycle), and this effect was neglected in our model. This phenomenon could nevertheless explain our findings, through an enhancement of the mean laser field that would be, according to our results, of a factor of ~ 30 and 20 in the case of argon and krypton clusters respectively. It must also be emphasized that in our model, the ionization thresholds are taken to be those of *isolated* ions, whereas this may not be the case inside the cluster.

6. CONCLUSION

KeV X-ray production from irradiation of large rare-gas clusters by intense ultrashort laser pulses has been quantitatively studied. Variation laws with laser intensity, cluster size and atomic species have been obtained. A simple model taking into account the inner-shell ionization induced by the laser-driven electron motion reproduces well the observed dependence and the absolute photon yields for the high intensity measurements. However, new measurements have shown that the threshold behavior embedded in our model is not as simple as expected. Next experiments will test the X-ray yield dependence on the laser wavelength and polarization. Future measurements will also be performed at shortest working distance from the nozzle, thus increasing the cluster target density. Our results and their interpretation suggest that X-ray emission may occurs on a very short time scale (a few hundreds fs), and time resolved measurements are also planned. The production of subpicosecond pulses of 10^{11} photons per laser pulse in the keV range seems to be at hand, and numerous applications may be foreseen.

ACKNOWLEDGEMENTS

The authors acknowledge the efficient support of the LUCA technical staff: M. Bougeard and E. Caprin, for skilled technical assistance.

REFERENCES

1. Shao, Y. L. *et al.*, Phys. Rev. Lett. **77**, 3343 (1996)
2. Purnell, J. *et al.*, Chem. Phys. Lett. **229**, 333 (1994)
3. Snyder, E. M. *et al.*, Phys. Rev. Lett. **77**, 3347 (1996)
4. Lezius, M. *et al.*, J. Phys. B : At. Mol. Opt. Phys. **30**, L251 (1997)
5. Ditmire, T. *et al.*, Nature **386**, 54 (1997)
6. Wülker, C. *et al.*, Opt. Commun. **112**, 21 (1994)
7. McPherson, A. *et al.*, Phys. Rev. Lett. **72**, 1810 (1994)
8. Ditmire, T. *et al.*, Phys. Rev. Lett. **75**, 3122 (1995); Ditmire, T. *et al.*, Phys. Rev. A **53**, 3379 (1996)
9. Dobosz, S. *et al.*, Phys. Rev. A **56**, R1 (1997)
10. Lezius, M. *et al.*, OSA VIIth proceeding, Santa Fe (USA) (1997)
11. Kondo, K. *et al.*, J. Phys. B : At. Mol. Opt. Phys. **30**, 2707 (1998)
12. Ditmire, T. *et al.*, J. Phys. B : At. Mol. Opt. Phys. **31**, 2825 (1998)
13. Rose-Petruck, C. *et al.*, Phys. Rev. A **55**, 1182 (1997)
14. Vernhet, D. *et al.*, J. Phys. B : At. Mol. Opt. Phys. **31**, 3949 (1998)
15. Hagena, O. F. and Obert W., J. Chem. Phys. **56**, 1793 (1972)
16. Augst, S. *et al.*, Phys. Rev. Lett. **63**, 2212 (1989)
17. Bhalla, C. P., Phys. Rev. A **8**, 2877 (1973)
18. Cornille, M., Private communication.
19. Klapisch, M., Comp. Phys. Comm., **2**, 239 (1971); Klapisch, M., Schwob, J.L., Fraenkel, B.S. and Oreg, J., J. Opt. Soc. Am., **67**, 148 (1977); Bar-Shalom, A., Klapisch, M. and Oreg, J., Phys. Rev. A **38**, 1773 (1988)
20. Moshhammer, R. *et al.*, Phys. Rev. Lett. **84**, 447 (2000)
21. Dobosz, S., These de doctorat Université Paris 13. (1998)
22. Hippler, R. and Jitschin, W., Z. Phys. A **307**, 287 (1982)